

# Naming the Concepts Classifiers Rely On: Language-Anchored Decomposition for Faithful Explanation

Ahsan Habib Akash<sup>1</sup> Dipkamal Bhusal<sup>2</sup> Stacey Jones<sup>3</sup>  
Donald A. Adjeroh<sup>1</sup> Binod Bhattarai<sup>4,5,6</sup> Prashnna Kumar Gyawali<sup>1\*</sup>

<sup>1</sup>West Virginia University, USA <sup>2</sup>Rochester Institute of Technology, USA <sup>3</sup>O Analytics

<sup>4</sup>University of Aberdeen, UK <sup>5</sup>Fogsphere (Redev.AI Ltd, UK)

<sup>6</sup>University College London, UK

## Abstract

Deep neural networks are widely deployed in high-stakes visual applications where interpretability is critical, yet existing explanations face a trade-off: post-hoc concept methods recover factors that are faithful to a model’s behavior but unnamed, while naming and by-design methods attach human-readable concepts only by retraining or altering the classifier. We propose Language-Anchored Decomposition (LAD), a post-hoc framework that delivers concepts which are simultaneously named, faithful, and obtained without modifying the model. For each class, a large language model proposes a concept vocabulary that CLIP-based similarity maps localize across image regions. Inverting standard non-negative matrix factorization, LAD fixes these language-grounded maps as the coefficient matrix and learns only a concept basis that reconstructs the frozen encoder’s activations, so naming becomes a structural constraint and the model’s own feature geometry determines which concepts are retained. Removing this anchor preserves accuracy but collapses attribution faithfulness. Across natural-image, scene, and medical-imaging benchmarks, LAD produces spatially precise explanations that are decision-relevant under both concept insertion and deletion, while uniquely providing stable, human-interpretable concept names. Code is available at: <https://github.com/machine-intelligence-lab-wvu/LAD>.

## 1. Introduction

Interpreting the decision mechanisms of deep visual models is crucial for diagnosing failures, mitigating biases, and ensuring responsible deployment in high-stakes applications. Post-hoc attribution methods such as Grad-CAM [20] and



Figure 1. Qualitative illustration of LAD. Each image is decomposed into spatially localized, named concepts, including part-level object concepts (e.g., “Pointy Ears,” “Green Eyes”) and contextual scene concepts (e.g., “Crowd in the Background,” “Player Dribbling”). Because each concept is anchored to language before decomposition, the explanations are both human-interpretable and faithful to the frozen classifier’s predictions.

Integrated Gradients [24] visualize the input regions most influential to a prediction, but they operate at the pixel level and emphasize low-level activations rather than the high-level cues humans reason with, offering limited semantic insight into a model’s decision process [14]. Concept-based explanations address this by attributing predictions to human-interpretable units such as object parts and visual attributes [6, 7, 9].

Existing concept-based methods, however, fall into two families that each pay a price. The first is *post-hoc concept discovery*. Building on TCAV [9], unsupervised methods such as ACE [7], ICE [28], and CRAFT [6] extract concepts via clustering or Non-Negative Matrix Factorization (NMF), and FACE [3] further aligns the decomposition with classifier logits to improve faithfulness. These methods are faithful to the model, but the recovered factors are unnamed: the same factor index can correspond to different visual elements across images, so a human must label each

\*Corresponding author: prashnna.gyawali@mail.wvu.edu

factor after the fact and consistency is not guaranteed. The second family attaches names directly. Concept Bottleneck Models [10], their label-free variants [16], and spatial extensions such as Show and Tell [2] predict named concepts before classification, while neuron-naming methods such as LaViSE [27] train an auxiliary explainer to describe individual filters. These methods produce names, but at a cost: by-design models replace the classifier head with a newly trained predictor, so the explained model is no longer the deployed one [19], and neuron-naming methods describe units without testing whether the named concepts are actually responsible for predictions. No prior method delivers concepts that are simultaneously *named*, *faithful*, and obtained *without modifying the model*.

We fill this gap with Language-Anchored Decomposition (LAD) by inverting the standard decomposition. For each target class, a large language model proposes a class-specific concept vocabulary; for “*cat*”, the proposals may include “pointy ears,” “green eyes,” and “whiskers.” We then use CLIP [18] image–text similarity to localize each concept across image regions. Rather than learning latent coefficients as in NMF, LAD *fixes* these language-grounded similarity maps as the coefficient matrix and learns only a concept basis that reconstructs the frozen encoder’s activations. Naming therefore becomes a structural constraint rather than a post-hoc label, and the model’s own feature geometry, not CLIP alone, determines which named concepts are retained. LAD needs no auxiliary training and no concept annotations, and tests faithfulness by reconstruction rather than describing units in isolation.

Crucially, the language anchor is not cosmetic. Replacing the fixed language-grounded coefficients with learned ones, which recovers standard unsupervised NMF on the same activations, preserves classification accuracy but sharply reduces attribution faithfulness. (Sec. 5.5). The anchor changes *which* basis directions are discovered, steering them toward classifier-meaningful structure, and the reconstruction objective reshapes the initial CLIP similarities so that concepts inconsistent with the encoder’s evidence are suppressed, mitigating known biases in CLIP-style models. Fig. 1 illustrates the resulting explanations, which recover fine-grained part-level concepts (top) and higher-level scene structure (bottom), each localized and paired with a natural-language name.

#### Main Contributions:

- A post-hoc concept discovery framework, Language-Anchored Decomposition (LAD), that inverts NMF by fixing language-grounded CLIP similarity maps as the coefficient matrix and learning only the concept basis against frozen encoder activations. Naming is enforced structurally, with no retraining and no manual concept annotations.
- Evidence that the language anchor is functional rather

than cosmetic: removing it preserves accuracy but collapses deletion faithfulness, showing that language supervision determines which concept directions are discovered.

- Evaluation across natural-image, scene, and medical benchmarks showing that LAD’s named concepts are decision-relevant under concept insertion and deletion, at faithfulness comparable to the strongest prior method.

## 2. Related Work

Interpretability methods fall into two broad approaches: *post-hoc* methods that interpret a model after training, and *ante-hoc* explanation-by-design architectures that constrain the model during learning.

**Feature attribution:** Saliency maps [22], Grad-CAM [20], Integrated Gradients [24], and perturbation-based variants [17, 23] attribute importance to input pixels. These pixel-level maps lack semantic interpretability and can be visually plausible yet unfaithful to the model’s decision [5, 14].

**Post-hoc concept discovery:** TCAV [9] quantifies sensitivity to user-defined concepts but needs manual annotation, while ACE [7], ICE [28], and CRAFT [6] automate discovery via clustering or Non-negative Matrix Factorization (NMF). FACE [3] improves faithfulness with a KL regularizer aligning reconstructed and original predictions. These methods are faithful but their factors are *unnamed*: a factor index may map to different visual elements across images, so each must be labeled after the fact with no consistency guarantee.

**Naming individual units:** A parallel line attaches language to model internals at the level of individual neurons or filters: Network Dissection [1] via overlap with annotated concept masks, and MILAN [8] and CLIP-Dissect [15] via open-vocabulary descriptions of top-activating regions. LaViSE [27] maps masked filter activations to a semantic space to describe filters, including unseen concepts. These methods differ from ours on two axes. First, granularity: they name single units, whereas decomposition-based discovery, including LAD, recovers concepts as *directions* in activation space (combinations of units), the unit at which NMF-style methods operate. Second, faithfulness: they produce *descriptive* labels without testing whether a named concept is causally responsible for a prediction, and several [1, 8, 27] further require dense annotations or a trained explainer.

**Concept bottleneck and by-design models:** Concept Bottleneck Models and their label-free and spatial variants [2, 10, 12, 16, 26] predict named concepts before the output, recently using vision–language models to avoid manual labels. They are interpretable by construction but replace the classifier head with a newly trained predictor, so the explained model is no longer the deployed one [19].

**Our position:** Post-hoc discovery is faithful but unnamed, unit-naming provides names without verifying predictive responsibility, and by-design models attach names only by retraining. LAD occupies the intersection these families leave open: named, faithful, and obtained without modifying the model, by fixing language-grounded coefficients and learning the basis against the frozen encoder.

### 3. Methodology

An overview of LAD is shown in Fig. 2. We describe it beginning with the problem setup.

#### 3.1. Setup

A pretrained model maps inputs from an image space  $\mathcal{X} \subset \mathbb{R}^{3 \times H \times W}$  to predictions in  $\mathcal{Y} \subset \mathbb{R}^c$ . We decompose it into an *encoder*  $f: \mathcal{X} \rightarrow \mathbb{R}^{p \times h \times w}$  that produces spatial feature maps and a *classifier head*  $g: \mathbb{R}^p \rightarrow \mathbb{R}^c$  on globally pooled features. Both remain *frozen*: LAD explains the deployed model without retraining. For a batch of  $n$  inputs  $\mathbf{X}$ , the encoder produces

$$\mathbf{Z} = f(\mathbf{X}) \in \mathbb{R}^{n \times p \times h \times w},$$

where  $p$  is the channel dimension and  $(h, w)$  the spatial resolution. Global average pooling (GAP) over the spatial dimensions yields sample-wise latents, with predictions  $g(\mathbf{A})$ :

$$\mathbf{A} = \text{GAP}(\mathbf{Z}) \in \mathbb{R}^{n \times p}.$$

**Post-hoc Concept Discovery:** Given a frozen model  $g \circ f$ , post-hoc concept discovery seeks a low-dimensional, non-negative factorization of the latents  $\mathbf{A}$  into a small set of interpretable components. Most methods operate on pooled activations  $\mathbf{A}$ , restricting analysis to a single class to avoid cross-class confounds. Non-negative Matrix Factorization (NMF) is the common formulation:

$$\mathbf{A} \approx \mathbf{U}\mathbf{W}^\top, \quad \mathbf{U} \in \mathbb{R}_+^{n \times r}, \quad \mathbf{W} \in \mathbb{R}_+^{p \times r},$$

where  $r$  is the number of concepts. Each column of  $\mathbf{W}$  defines a concept direction in feature space, and the matching column of  $\mathbf{U}$  its per-sample activation strength. Reconstructed features  $\hat{\mathbf{A}} = \mathbf{U}\mathbf{W}^\top$  can be passed through  $g(\cdot)$  to assess predictive consistency.

#### 3.2. Semantically Anchored Matrix Factorization

Unlike methods that factorize globally pooled representations  $\mathbf{A} \in \mathbb{R}^{n \times p}$ , we factorize directly in the encoder’s spatial feature space to preserve localized evidence. We unfold the activations  $\mathbf{Z}$  over spatial and batch dimensions:

$$\bar{\mathbf{A}} = \text{Unfold}(\mathbf{Z}) \in \mathbb{R}^{(nhw) \times p},$$

so each row is a spatial location and each column a feature channel. Pooling before factorization implicitly assumes

concepts are spatially homogeneous across an image; unfolding instead treats each location as an independent observation, raising the effective sample size from  $n$  to  $nhw$  and capturing localized, part-level structure that pooling would average out. Concept discovery thus becomes a structured clustering over spatial feature vectors while remaining consistent with the classifier’s global decision pipeline.

**Inverting the Coefficient Matrix:** Standard NMF,  $\mathbf{A} \approx \mathbf{U}\mathbf{W}^\top$ , learns both  $\mathbf{U}$  and  $\mathbf{W}$ , so the coefficients  $\mathbf{U}$  are unconstrained and lack semantic alignment. We invert this: rather than discovering factors and labeling them afterward, we *fix* the coefficients to a semantically grounded matrix  $\mathbf{S}$  from language–vision similarity and learn only the basis,

$$\hat{\mathbf{A}} \approx \mathbf{S}\mathbf{W}^\top, \quad \mathbf{S} \in \mathbb{R}_+^{(nhw) \times r}.$$

Each column of  $\mathbf{S}$  is a human-interpretable concept and each entry the similarity between a spatial location and a concept prompt. This turns factorization into a semantically constrained reconstruction: we learn a basis  $\mathbf{W}$  that best reconstructs encoder activations under fixed, language-aligned coefficients. Because the concept identity is fixed a priori by  $\mathbf{S}$ , each basis vector is tied to a named concept, and naming becomes a structural property of the factorization rather than a post-hoc step.

#### 3.3. Language-Anchored Concept Map Construction

**Class-Specific Concept Vocabulary:** For each class  $c \in \mathcal{C}$  we build a fixed-size vocabulary  $\mathcal{T}_c = \{t_1, \dots, t_r\}$  of visually grounded concepts ( $r = 25$  unless noted; sensitivity in Sec. 5.5). Following [16], we prompt a large language model with structured templates eliciting diverse attributes (object parts, textures, shapes, materials, poses, contextual cues). Automatic filtering removes (i) generic filler terms (e.g., “object”), (ii) concepts overlapping the class name (preventing trivial leakage), and (iii) near-duplicates by CLIP text-embedding similarity, yielding a compact, diverse vocabulary with no manual annotation. Templates and filtering details are in the supplement.

**Localized CLIP Similarity Maps:** Given an image  $x_n$  and its vocabulary  $\mathcal{T}_c$ , we construct spatial concept maps via localized prompting [2, 21]. After CLIP’s deterministic pre-processing, we define a grid aligned to  $(h, w)$  and, at each location, form a variant  $x_n^{(h,w)}$  by overlaying a small red circle. With  $\ell_2$ -normalized CLIP encoders  $E_I, E_T$ , the cosine similarity for concept  $t_m$  is

$$s_{n,m}^{(h,w)} = \frac{E_I(x_n^{(h,w)}) \cdot E_T(\text{'a photo of } t_m\text{'})}{\|E_I(x_n^{(h,w)})\|_2 \|E_T(\text{'a photo of } t_m\text{'})\|_2}.$$

This gives a spatial map  $s_{n,m} \in \mathbb{R}^{h \times w}$ ; flattening yields  $\mathbf{s}_n \in \mathbb{R}^{(hw) \times r}$  per image, and stacking across images forms

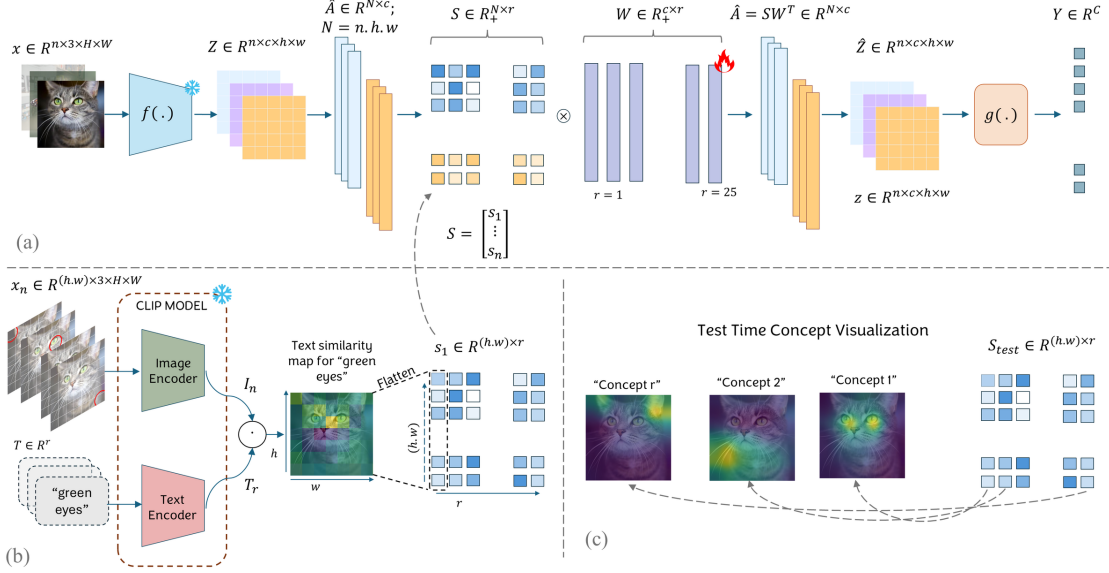


Figure 2. **LAD framework.** (a) An input image is processed through a pretrained encoder  $f(\cdot)$  to obtain latent activation maps, divided into spatial patches and arranged into a matrix  $\hat{\mathbf{A}} \in \mathbb{R}^{N \times c}$ . (b) Using CLIP-based semantic priors, the concept similarity matrix  $\mathbf{S}$  is *fixed* as the coefficient matrix while the basis  $\mathbf{W}$  is learned through a language-anchored reconstruction  $\hat{\mathbf{A}} \approx \mathbf{S}\mathbf{W}^\top$ ; the reconstructed activations preserve spatial coherence and predictive alignment with the classifier head  $g(\cdot)$ . (c) At inference, the estimated concept activations yield interpretable spatial maps and class-specific concept importance vectors.

the fixed coefficient matrix

$$\mathbf{S} = [\mathbf{s}_1; \dots; \mathbf{s}_n] \in \mathbb{R}^{(nhw) \times r},$$

whose rows are spatial locations and columns named concepts, used in the reconstruction  $\hat{\mathbf{A}} \approx \mathbf{S}\mathbf{W}^\top$ .

### 3.4. Activation-Level Reconstruction Optimization

With  $\mathbf{S}$  fixed, we recover the concept basis by minimizing the reconstruction error

$$\min_{\mathbf{W} \geq 0} \mathcal{L}_{\text{recon}} = \frac{1}{2} \|\bar{\mathbf{A}} - \mathbf{S}\mathbf{W}^\top\|_F^2. \quad (1)$$

Since GAP is linear and the head reads only pooled features, a small reconstruction error in  $\bar{\mathbf{A}}$  bounds the perturbation of  $\mathbf{A}$ , and hence of the logits; empirically, minimizing Eq. 1 alone preserves accuracy across datasets and backbones without output-level regularization. Unlike prior approaches that jointly learn both factors or regularize logits, we fix  $\mathbf{S}$  and learn only  $\mathbf{W}$ , enforcing semantic alignment structurally rather than through auxiliary losses.

We optimize Eq. 1 with projected gradient descent (PGD) to enforce non-negativity:

$$\mathbf{W} \leftarrow \max(0, \mathbf{W} - \eta \nabla_{\mathbf{W}} \mathcal{L}_{\text{recon}}), \quad (2)$$

initialized with NNDSVD [4]. With  $\mathbf{S}$  fixed the objective is smooth in  $\mathbf{W}$  and PGD converges to a stationary point (supplement).

### 3.5. Inference via Non-Negative Semantic Coefficient Estimation

With the basis  $\mathbf{W}$  learned, we explain a new image  $x$  against the same frozen encoder. We extract and unfold its activations to  $\bar{\mathbf{A}} \in \mathbb{R}^{(hw) \times p}$  and, with  $\mathbf{W}$  fixed, estimate non-negative coefficients  $\hat{\mathbf{S}} \in \mathbb{R}_+^{(hw) \times r}$  by non-negative least squares:

$$\min_{\hat{\mathbf{S}} \geq 0} \frac{1}{2} \|\hat{\mathbf{S}}\mathbf{W}^\top - \bar{\mathbf{A}}\|_F^2. \quad (3)$$

A fast non-negative initialization is the projected normal equation

$$\hat{\mathbf{S}}_0 = \text{ReLU}(\bar{\mathbf{A}}\mathbf{W}(\mathbf{W}^\top\mathbf{W})^{-1}), \quad (4)$$

optionally refined by projected gradient descent,

$$\hat{\mathbf{S}} \leftarrow \text{ReLU}\left(\hat{\mathbf{S}} - \eta(\hat{\mathbf{S}}\mathbf{W}^\top\mathbf{W} - \bar{\mathbf{A}}\mathbf{W})\right), \quad (5)$$

with  $\eta$  from the spectral norm of  $\mathbf{W}^\top\mathbf{W}$ . The reconstruction  $\hat{\mathbf{A}} = \hat{\mathbf{S}}\mathbf{W}^\top$  is then reshaped and passed through the head after pooling; predictive preservation is the accuracy of the original versus reconstructed activations.

### 3.6. Concept Heatmaps and Visualization

We project the inferred coefficients back to the spatial domain. Reshaping  $\hat{\mathbf{S}}$  to  $\hat{\mathbf{S}}_{\text{spatial}} \in \mathbb{R}^{h \times w \times r}$ , each concept  $k$  gives a normalized heatmap

$$\mathbf{M}_k = \text{Normalize}\left(\hat{\mathbf{S}}_{\text{spatial}}(:, :, k)\right), \quad (6)$$

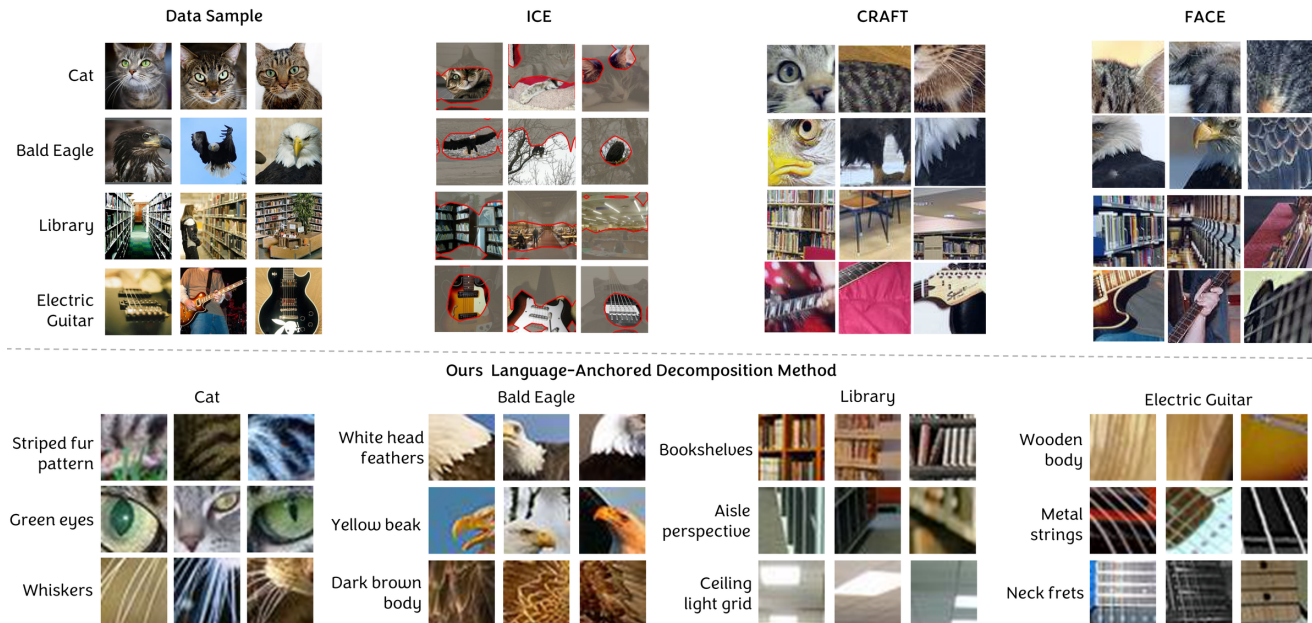


Figure 3. Concept discovery results on ImageNet. The upper panel shows top-ranked concepts from NMF baselines (ICE, CRAFT, FACE), which highlight coarse regions without semantic names; the lower panel shows LAD, which produces fine-grained, spatially coherent concepts each paired with a human-interpretable name.

rescaled to  $[0, 1]$ , highlighting regions whose features are best reconstructed by the  $k$ -th basis vector. Overlaid on the image, and since channel  $k$  corresponds to the named concept  $t_k$  (e.g., “pointy ears”), each map is a semantically grounded explanation of localized evidence.

## 4. Experimental Setup

**Datasets:** We evaluate LAD on ImageNet (ILSVRC 2012) using a publicly available pretrained ResNet34, analyzing 500 of the 1,000 classes, a substantial expansion over prior concept-discovery work that reports on as few as 10 classes [3]. For scene-centric generalization we use Places365-Standard with the publicly available pretrained ResNet50 checkpoint, covering 364 of 365 categories (one excluded due to 0% baseline accuracy). We also evaluate a clinical domain (Sec. 5.4); additional analyses, including results on further CNN backbones and a Vision Transformer case study, are provided in the supplementary material.

**Baselines:** We compare against representative NMF-based concept discovery methods: ICE [28], CRAFT [6], and FACE [3], all using identical backbones, preprocessing, data splits, and concept counts  $r$ .

**Metrics:** **Acc** is top-1 agreement between predictions on original and reconstructed activations. **C-Ins** ( $\uparrow$ ) measures whether concepts are *sufficient* for the decision (performance restored as top concepts are inserted), and **C-Del** ( $\uparrow$ ) whether they are *necessary* (performance degraded as they are removed).

## 5. Results

### 5.1. Named Concepts and Per-Image Rollouts

Because LAD anchors each factor to a language-defined concept, a concept refers to the same entity wherever it appears: *maple neck*, *fretted scale*, and *tuning pegs* localize to the same parts across every image of the *Electric Guitar* class. NMF baselines (ICE, CRAFT, FACE) recover *unnamed* factors, so the same factor index may highlight the guitar body in one image and the fretboard in another, limiting cross-image comparability [11, 13]. Figure 3 contrasts the two: baseline factors highlight coarse or discriminative regions with no name, whereas LAD recovers fine-grained concepts each tied to a human-interpretable label.

This naming enables a capability no baseline provides: the *per-image named-concept rollout*. For a single input, LAD returns the named concepts the model used, each localized, ranked by importance, and annotated with its contribution to the reconstruction,

$$\hat{c}_k = \frac{\|\hat{\mathbf{S}}[:, k]\|_2 \|\mathbf{W}[:, k]\|_2}{\sum_j \|\hat{\mathbf{S}}[:, j]\|_2 \|\mathbf{W}[:, j]\|_2}, \quad (7)$$

the share of the reconstruction explained by concept  $k$ ; the baselines can only emit “factor 1, factor 2, ...” for a human to label afterward. Figure 4 (top) shows this for an electric guitar and an axolotl: LAD returns localized, named concepts with their contributions, while FACE returns factors of comparable contribution but no semantic label.

Table 1. Primary comparison across datasets. All methods preserve accuracy, so faithfulness is read from concept insertion (C-Ins) and deletion (C-Del): LAD leads on insertion and uniquely names its concepts, while FACE is strongest on deletion. Best per column within each panel in bold.

Method	Acc $\uparrow$	C-Ins $\uparrow$	C-Del $\uparrow$
<i>ImageNet (ResNet34, 500 cls)</i>			
LAD	<b>1.000</b>	<b>0.973</b>	0.902
FACE	0.998	0.952	<b>0.939</b>
CRAFT	0.976	0.918	0.808
ICE	0.997	0.907	0.545
<i>Places365 (ResNet50, 364 cls)</i>			
LAD	<b>1.000</b>	<b>0.972</b>	0.880
FACE	0.994	0.925	<b>0.919</b>
CRAFT	0.947	0.868	0.828
ICE	0.995	0.887	0.631

Naming also yields *cross-image consistency* that unnamed factors lack. Figure 4 (bottom) tracks one LAD concept, *maple neck*, against FACE’s leading factor across several images of the class: the named concept localizes to the neck in every image, whereas the unnamed factor attaches to a different region each time, so its meaning cannot be read off the index. The rollout is thus the per-image, named view of the structure our aggregate metrics summarize (Tab. 1): the concepts it surfaces are those whose insertion and deletion move the prediction.

## 5.2. Predictive Preservation and Faithful Attribution

Table 1 reports our primary comparison. All methods preserve accuracy on both ResNet backbones, with LAD highest, so the semantic constraints do not distort the classifier’s representations; with Acc saturated, faithfulness is read from insertion and deletion. LAD attains the highest C-Ins on both datasets, so its named concepts are the most efficient at restoring the prediction. On C-Del, FACE is strongest. This ordering reflects a design difference, not a deficiency: FACE jointly optimizes coefficients and basis against classifier logits, absorbing any decision-relevant direction including non-interpretable ones, whereas LAD fixes the coefficients to named concepts and recovers a semantically constrained *subset* of decision-relevant evidence. Trading a portion of deletion completeness for named, verifiable concepts is the intended behavior, and the gap narrows as the concept budget grows (Sec. 5.5).

**Computational cost:** LAD is also cheaper to fit than the jointly-optimized baselines. Fixing  $\mathbf{S}$  reduces concept learning to a single non-negative least-squares solve for  $\mathbf{W}$ , avoiding the alternating factor updates of CRAFT and the

logit-regularized optimization of FACE. On an RTX A4500, LAD fits a class in 0.03 s, versus 0.5 s (CRAFT) and 2.6 s (FACE); a one-time LLM concept generation step adds  $\sim 15$  s/class. A full complexity and wall-clock analysis is in the supplement.

## 5.3. The Model’s Geometry Determines Retained Concepts

A central claim of LAD is that the frozen encoder, not CLIP, determines which named concepts survive. Figure 6 provides direct evidence: before optimization, concept scores reflect the CLIP initialization and rank relatively uniformly; after optimizing the basis against encoder activations, the distributions disperse as coefficients are reshaped to reconstruct the model’s internal features. Concepts inconsistent with the encoder’s evidence receive small basis weight and are suppressed, so LAD retains only concepts causally aligned with the decision, which matters given known biases in CLIP-style models [25].

## 5.4. Concepts in a Clinical Domain

To test whether LAD produces decision-relevant named concepts where interpretability carries real stakes, we evaluate on retinal fundus photographs (ODIR-5K, five ocular-disease classes). The explained model is a DenseNet-121 fine-tuned to 0.755 balanced accuracy; per-class vocabularies are generated as disease-specific attributes (e.g., *bright exudate flecks*, *vascular dilation*, *drusen-like structures*) and localized with BiomedCLIP. Dataset and training details are in the supplement.

As on natural images, Acc and C-Ins saturate, so faithfulness is read from deletion (C-Del), where LAD is the most causally decisive of any method (Tab. 2). Unlike the natural-image setting, where FACE’s joint optimization edges out LAD on deletion, the clinical backbone’s evidence is spatially focal: disease signatures occupy small, localized regions rather than distributed texture. LAD’s named concepts anchor to these regions, so removing them degrades the prediction more sharply, and LAD leads C-Del by a wide margin (0.954 vs. 0.863). This aligns with our central finding that the encoder’s geometry, not the language prompts, determines which concepts are retained (Sec. 5.3): focal disease evidence aligns with named anatomical concepts.

Figure 5 shows the qualitative counterpart. For diabetic retinopathy, LAD separates the prediction into named concepts localized to distinct regions; for age-related macular degeneration, *drusen-like structures* localizes to the yellow deposits temporal to the optic disc, a hallmark of the disease. Because each map carries a clinical name, a reader inspects not only *where* the model looks but *what* it attributes there, and can flag when the two disagree, making the rollout an auditable record of the model’s evidence rather than

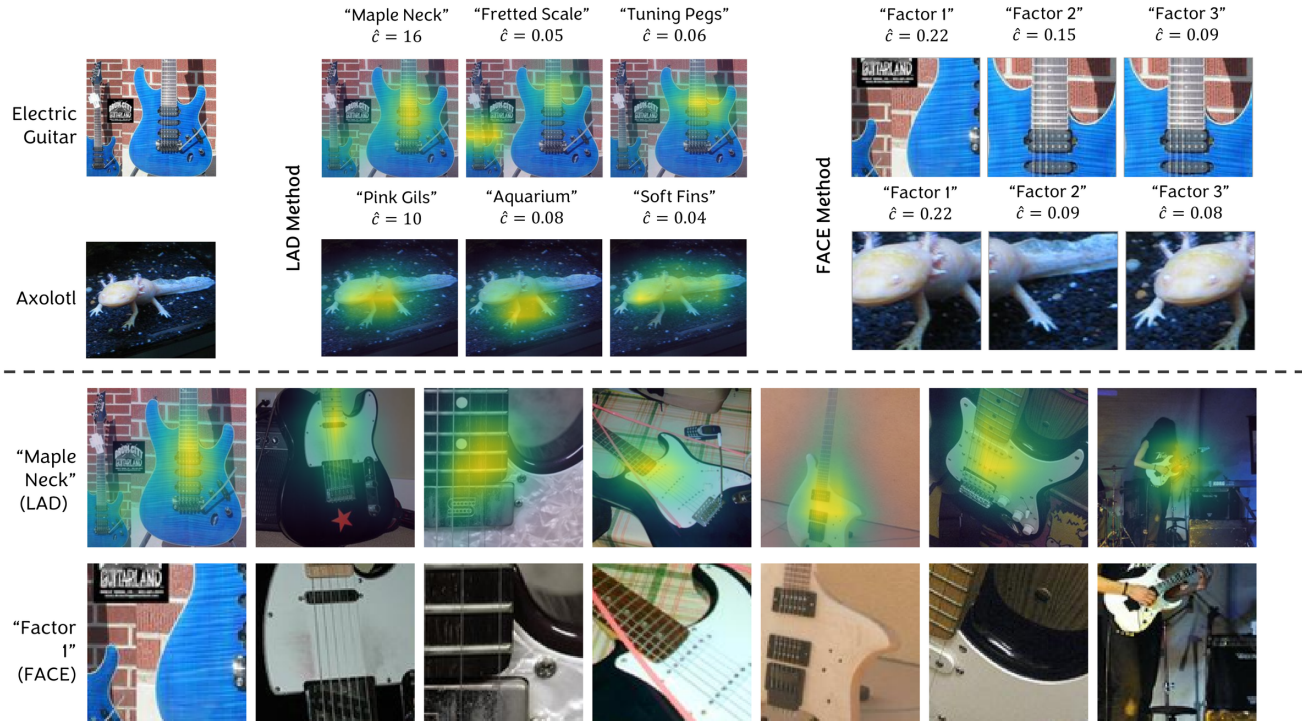


Figure 4. **Per-image named-concept rollouts, a capability unique to LAD.** **Top:** for an electric guitar ( $p=0.99$ ) and an axolotl ( $p=1.00$ ), LAD returns localized, *named* concepts with their reconstruction contribution  $\hat{c}$  (Eq. (7)); FACE returns factors of comparable contribution but with no semantic label (Factor 1–3). **Bottom:** the same named concept (*maple neck*) localizes to the neck across different images of the class, whereas FACE’s leading factor (Factor 1) attaches to a different region in each image, so its meaning is not consistent across images. Examples are the median-C-Ins image per class, fixed in advance.

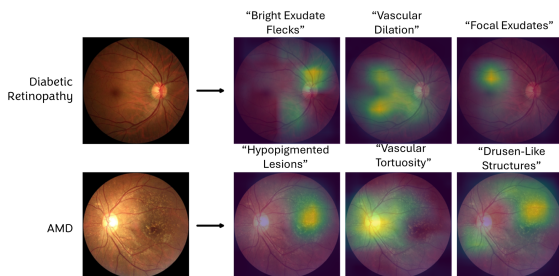


Figure 5. **Named-concept rollouts on retinal fundus images.** For a diabetic retinopathy case (top) and an age-related macular degeneration case (bottom), LAD decomposes the prediction into separately named, localized concepts. Each map is anchored to a clinical term, so the explanation reports both where the model looks and what it attributes to that region. Two representative classes are shown; per-disease results are in the supplement.

an unlabeled saliency map.

### 5.5. Ablation Studies

**The language anchor:** Table 3 replaces the fixed language-grounded coefficients  $\mathbf{S}$  with learned ones (standard unsupervised NMF on the same  $\mathbf{\tilde{A}}$ ). Accuracy is unchanged,

Table 2. Concept faithfulness on retinal fundus (DenseNet-121 @448, BiomedCLIP), mean over the four disease classes (normal excluded). Acc and C-Ins saturate; methods separate on C-Del, where LAD leads by a wide margin. All metrics  $\uparrow$ ; best in bold. Per-disease results are in the supplement.

Method	Acc	C-Ins	C-Del
LAD (ours)	<b>1.000</b>	<b>0.980</b>	<b>0.954</b>
FACE	0.990	0.980	0.863
CRAFT	1.000	0.980	0.850
ICE	0.990	0.980	0.455

but removing the anchor collapses deletion faithfulness, dropping C-Del from 0.902 to 0.507. The anchor changes *which* basis directions are discovered, steering them toward classifier-meaningful structure that a purely data-driven factorization does not recover.

**Effect of concept budget  $r$ :** Table 4 varies the number of concepts per class. Accuracy is saturated at all  $r$ , while C-Ins and C-Del improve monotonically: a larger vocabulary yields a more expressive basis that remains predictively faithful. We fix  $r = 25$  in the main experiments to match the baselines’ budgets; larger  $r$  trades a modest gain in deletion

Table 3. The language anchor is functional, not cosmetic. Replacing fixed language-grounded coefficients with learned ones leaves accuracy unchanged but sharply reduces deletion faithfulness (C-Del). ImageNet, ResNet34, 500 classes,  $r=25$ , identical splits. All metrics  $\uparrow$ .

Variant	Acc	C-Ins	C-Del
LAD (fixed $\mathbf{S}$ )	<b>1.000</b>	<b>0.973</b>	<b>0.902</b>
Unsupervised NMF on $\bar{\mathbf{A}}$	1.000	0.942	0.507
$\Delta$ (language)	—	+0.031	+0.395

Table 4. Effect of concept budget  $r$ . Accuracy is saturated; faithfulness improves monotonically with  $r$ . ImageNet, ResNet34, 500 classes.

$r$	Acc $\uparrow$	C-Ins $\uparrow$	C-Del $\uparrow$	MSE $\downarrow$
10	1.000	0.941	0.860	1.477
25	1.000	0.973	0.902	1.483
50	1.000	0.985	0.953	1.543
100	1.000	0.992	0.956	1.382

faithfulness for reduced per-image interpretability.

## 6. Conclusion

We introduced LAD, a post-hoc framework that produces concepts which are simultaneously named, faithful, and obtained without modifying the model. By inverting non-negative matrix factorization, fixing CLIP-derived language-grounded coefficients and learning only the concept basis against the frozen encoder, LAD ties each basis direction to a human-readable concept while preserving the model’s predictive behavior. Removing the language anchor preserves accuracy but collapses faithfulness, showing that the anchor determines which concept directions are discovered rather than merely labeling them.

Across ImageNet and Places365, LAD matches the strongest prior method on faithfulness while uniquely supporting per-image named-concept rollouts: for a single input, the named concepts the model relied on, each localized and annotated with its contribution. On retinal fundus images its named concepts are the most causally decisive of any method, showing the approach carries to a high-stakes clinical domain. By making a model’s semantic evidence directly inspectable and comparable across images, LAD supports more transparent vision models where understanding the content of a decision matters as much as its accuracy.

## References

- [1] David Bau, Bolei Zhou, Aditya Khosla, Aude Oliva, and Antonio Torralba. Network dissection: Quantifying interpretability of deep visual representations. In *Proceedings of the IEEE Conference on Computer Vision and Pattern Recognition (CVPR)*, 2017. 2
- [2] Itay Benou and Tammy Riklin Raviv. Show and tell: Visually explainable deep neural nets via spatially-aware concept bottleneck models. In *Proceedings of the Computer Vision and Pattern Recognition Conference*, pages 30063–30072, 2025. 2, 3
- [3] Dipkamal Bhusal, Michael Clifford, Sara Rampazzi, and Nidhi Rastogi. Face: Faithful automatic concept extraction. *NeurIPS*, 2025. 1, 2, 5
- [4] Christos Boutsidis and Efstratios Gallopoulos. Svd based initialization: A head start for nonnegative matrix factorization. *Pattern Recognition*, 41(4):1350–1362, 2008. 4, 12
- [5] Julien Colin, Thomas Fel, Rémi Cadène, and Thomas Serre. What i cannot predict, i do not understand: A human-centered evaluation framework for explainability methods. *Advances in neural information processing systems*, 35: 2832–2845, 2022. 2
- [6] Thomas Fel, Agustin Picard, Louis Bethune, Thibaut Boissin, David Vigouroux, Julien Colin, Rémi Cadène, and Thomas Serre. Craft: Concept recursive activation factorization for explainability. In *Proceedings of the IEEE/CVF conference on computer vision and pattern recognition*, pages 2711–2721, 2023. 1, 2, 5
- [7] Amirata Ghorbani, James Wexler, James Y Zou, and Been Kim. Towards automatic concept-based explanations. *Advances in neural information processing systems*, 32, 2019. 1, 2
- [8] Evan Hernandez, Sarah Schwettmann, David Bau, Teona Bagashvili, Antonio Torralba, and Jacob Andreas. Natural language descriptions of deep visual features. In *International Conference on Learning Representations (ICLR)*, 2022. 2
- [9] Been Kim, Martin Wattenberg, Justin Gilmer, Carrie Cai, James Wexler, Fernanda Viegas, et al. Interpretability beyond feature attribution: Quantitative testing with concept activation vectors (tcav). In *International conference on machine learning*, pages 2668–2677. PMLR, 2018. 1, 2
- [10] Pang Wei Koh, Thao Nguyen, Yew Siang Tang, Stephen Mussmann, Emma Pierson, Been Kim, and Percy Liang. Concept bottleneck models. In *International conference on machine learning*, pages 5338–5348. PMLR, 2020. 2
- [11] Zachary C Lipton. The mythos of model interpretability: In machine learning, the concept of interpretability is both important and slippery. *Queue*, 16(3):31–57, 2018. 5
- [12] Max Losch, Mario Fritz, and Bernt Schiele. Interpretability beyond classification output: Semantic bottleneck networks. *arXiv preprint arXiv:1907.10882*, 2019. 2
- [13] Christoph Molnar, Gunnar König, Julia Herbringer, Timo Freiesleben, Susanne Dandl, Christian A Scholbeck, Giuseppe Casalicchio, Moritz Grosse-Wentrup, and Bernd Bischl. General pitfalls of model-agnostic interpretation methods for machine learning models. In *International Workshop on Extending Explainable AI Beyond Deep Models and Classifiers*, pages 39–68. Springer, 2020. 5
- [14] Giang Nguyen, Daeyoung Kim, and Anh Nguyen. The effectiveness of feature attribution methods and its correlation with automatic evaluation scores. *Advances in Neural Information Processing Systems*, 34:26422–26436, 2021. 1, 2

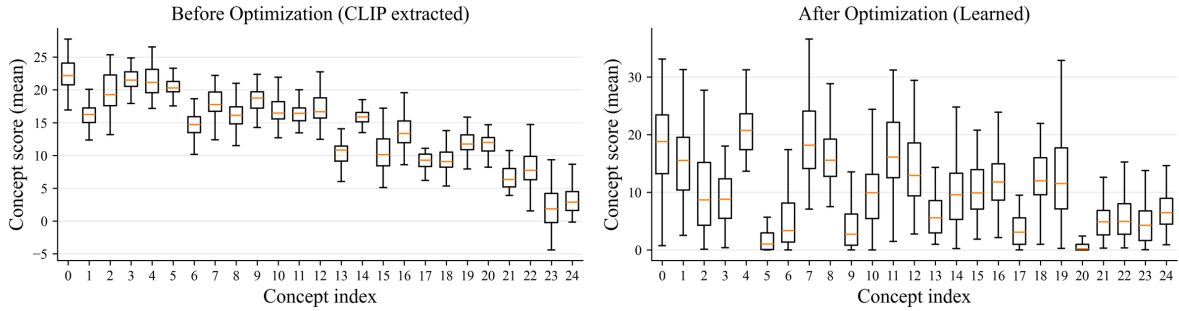


Figure 6. Concept activation scores before and after optimization, across 50 images. Before optimization, scores largely reflect the CLIP similarity initialization; after, the reconstruction objective reshapes them to match encoder activations, indicating the final concept maps are driven by the model’s internal representations rather than the initial CLIP similarity.

- [15] Tuomas Oikarinen and Tsui-Wei Weng. CLIP-Dissect: Automatic description of neuron representations in deep vision networks. In *International Conference on Learning Representations (ICLR)*, 2023. 2
- [16] Tuomas Oikarinen, Subhro Das, Lam M Nguyen, and Tsui-Wei Weng. Label-free concept bottleneck models. *International Conference on Learning Representations (ICLR)*, 2023. 2, 3
- [17] Vitali Petsiuk, Abir Das, and Kate Saenko. Rise: Randomized input sampling for explanation of black-box models. In *Proceedings of the British Machine Vision Conference (BMVC)*, 2018. 2
- [18] Alec Radford, Jong Wook Kim, Chris Hallacy, Aditya Ramesh, Gabriel Goh, Sandhini Agarwal, Girish Sastry, Amanda Askell, Pamela Mishkin, Jack Clark, et al. Learning transferable visual models from natural language supervision. In *International conference on machine learning*, pages 8748–8763. PmLR, 2021. 2
- [19] Cynthia Rudin. Stop explaining black box machine learning models for high stakes decisions and use interpretable models instead. *Nature machine intelligence*, 1(5):206–215, 2019. 2
- [20] Ramprasaath R Selvaraju, Michael Cogswell, Abhishek Das, Ramakrishna Vedantam, Devi Parikh, and Dhruv Batra. Grad-cam: Visual explanations from deep networks via gradient-based localization. In *Proceedings of the IEEE international conference on computer vision*, pages 618–626, 2017. 1, 2
- [21] Aleksandar Shtedritski, Christian Rupprecht, and Andrea Vedaldi. What does clip know about a red circle? visual prompt engineering for vlms. In *Proceedings of the IEEE/CVF International Conference on Computer Vision*, pages 11987–11997, 2023. 3
- [22] Karen Simonyan, Andrea Vedaldi, and Andrew Zisserman. Deep inside convolutional networks: Visualising image classification models and saliency maps. In *2nd International Conference on Learning Representations (ICLR)*, 2014. 2
- [23] Daniel Smilkov, Nikhil Thorat, Been Kim, Fernanda Viégas, and Martin Wattenberg. Smoothgrad: removing noise by adding noise. *arXiv preprint arXiv:1706.03825*, 2017. 2
- [24] Mukund Sundararajan, Ankur Taly, and Qiqi Yan. Axiomatic attribution for deep networks. In *International conference on machine learning*, pages 3319–3328. PMLR, 2017. 1, 2
- [25] Md Mehrab Tanjim, Krishna Kumar Singh, Kushal Kafle, Ritwik Sinha, and Garrison W Cottrell. Discovering and mitigating biases in clip-based image editing. In *Proceedings of the IEEE/CVF Winter Conference on Applications of Computer Vision*, pages 2984–2993, 2024. 6
- [26] Bowen Wang, Liangzhi Li, Yuta Nakashima, and Hajime Nagahara. Learning bottleneck concepts in image classification. In *Proceedings of the IEEE/CVF conference on computer vision and pattern recognition*, pages 10962–10971, 2023. 2
- [27] Yu Yang, Seungbae Kim, and Jungseock Joo. Explaining deep convolutional neural networks via latent visual-semantic filter attention. In *Proceedings of the IEEE/CVF Conference on Computer Vision and Pattern Recognition (CVPR)*, 2022. 2
- [28] Ruihan Zhang, Prashan Madumal, Tim Miller, Krista A. Ehinger, and Benjamin I. P. Rubinstein. Invertible concept-based explanations for cnn models with non-negative concept activation vectors. In *Proceedings of the AAAI Conference on Artificial Intelligence*, 2021. 1, 2, 5

# Supplementary Material

**Organization.** This supplementary material provides additional implementation details, theoretical analysis, and extended results supporting the main paper.

- Sec. A1 describes the construction of the class-specific concept vocabularies via LLM generation and semantic filtering, and the CLIP-based spatial probing used to build concept maps (Sec. A1.6).
- Sec. A2 gives the optimization solver details deferred from the main paper.
- Sec. A3 provides the convergence analysis for the projected gradient descent procedure.
- Sec. A4 evaluates four additional ImageNet backbones, including a robustness analysis on a lightweight network.
- Sec. A5 reports a second clinical domain (dermoscopy) and an analysis of where the discovered concepts localize.
- Sec. A6 reports a per-stage computational cost and memory analysis against the baselines.
- Sec. A7 presents a Vision Transformer case study.
- Sec. A8 shows extended qualitative visualizations of discovered concepts.
- Sec. A9 provides additional qualitative comparisons with ICE, CRAFT, and FACE.

## A1. Class-Specific Concept Vocabulary Generation

For each target class, we construct a fixed vocabulary of 25 visually grounded concepts that serve as the semantic basis for our concept maps. The vocabulary is generated using a constrained large language model (LLM) pipeline followed by lexical and CLIP-based semantic filtering.

### A1.1. Prompt Design

Concept proposals are generated using the `gpt-4o-mini` model. The system prompt instructs the model to generate short, visually grounded descriptors suitable for interpretability analysis. The user prompt specifies the target ImageNet class and enforces several constraints:

- Exactly 25 concepts must be generated.
- Each concept must contain 2–3 lowercase words.
- Concepts must describe visually grounded attributes such as parts, textures, shapes, contexts, or actions.
- The class name and trivial synonyms are disallowed.
- Previously rejected or accepted concepts are added to a banned list to encourage diversity across iterations.

Example prompt template:

```
Generate EXACTLY 25 distinct visual
concepts for the ImageNet class:
"{class_name}". Concepts must be 2-3
words, lowercase, visually grounded.
```

Avoid the class name or synonyms.  
Avoid generic words such as "object",  
"scene", "photo". Return JSON only.

### A1.2. Schema-Constrained Generation

To ensure structured, reproducible outputs, generation is constrained by a strict JSON schema: the output must contain the class name and exactly 25 concept strings,

$$\text{schema} = \begin{cases} \text{class\_name} : \text{string} \\ \text{concepts} : [c_1, \dots, c_{25}], \quad c_i \in \mathcal{S}, \end{cases} \quad (\text{A1})$$

where each concept  $c_i$  is a 2–3 word lowercase phrase of 3–40 characters matching the pattern

$$[a-z][a-z-]^*([ ] [a-z][a-z-]^*)\{1,2\}$$

This guarantees the LLM returns exactly 25 short, controlled-format concepts.

### A1.3. Stage-1 Lexical Filtering

Raw LLM outputs are normalized through lowercasing and removal of non-alphabetic characters. A rule-based filter then removes concepts that violate the following conditions:

- Not 2–3 words long
- Contain generic filler terms (e.g., *animal*, *object*, *scene*)
- Duplicate previously accepted concepts
- Contain tokens identical to the class name

To avoid removing meaningful attributes, we maintain a lexicon of visual attribute words spanning several categories:

- color (e.g., *yellow*, *black*)
- texture (e.g., *furry*, *shiny*)
- parts (e.g., *tail*, *wings*)
- shape (e.g., *long*, *round*)
- pose/motion (e.g., *running*, *flying*)
- environment (e.g., *forest*, *ocean*)
- material (e.g., *metal*, *wood*)

Concepts containing attribute words are preserved even if partial lexical overlap with the class name occurs.

### A1.4. Stage-2 CLIP Semantic Filtering

After lexical filtering, we apply a CLIP-based semantic filtering procedure to improve diversity and visual relevance.

Let  $t_i$  denote the CLIP text embedding of concept  $c_i$  obtained using the template:

“a photo of  $c_i$ ”.

If class images are available, we randomly sample up to 100 images from the target class and compute their CLIP image embeddings. The mean embedding

$$\mu_I = \frac{1}{N} \sum_{j=1}^N f_{\text{CLIP}}(I_j)$$

---

**Algorithm 1** Class-specific concept vocabulary generation

---

**Require:** class name  $c$ , LLM  $M$ , CLIP encoders  $f_{\text{text}}, f_{\text{img}}$   
**Require:** optional class images  $\mathcal{I}_c$ ; rounds  $R_{\text{clip}}=10, R_{\text{fb}}=5$   
**Ensure:** 25 filtered concepts  $\mathcal{K}$

- 1:  $\mathcal{K} \leftarrow \emptyset; \mathcal{B} \leftarrow \emptyset$  ▷ accepted; banned
- 2: **for**  $r = 1$  to  $R_{\text{clip}} + R_{\text{fb}}$  **do**
- 3:    $\mathcal{C} \leftarrow \text{LLMGENERATE}(M, c, \mathcal{B})$  ▷ 25 candidates
- 4:    $\mathcal{C} \leftarrow \text{LEXICALFILTER}(\mathcal{C}, c, \mathcal{K})$
- 5:   **if**  $r \leq R_{\text{clip}}$  **then**
- 6:      $\mathcal{C} \leftarrow \text{CLIPFILTERRANK}(\mathcal{C}, \mathcal{I}_c)$  ▷ skip in fallback
- 7:   **end if**
- 8:    $\mathcal{K} \leftarrow \mathcal{K} \cup \mathcal{C}; \mathcal{B} \leftarrow \mathcal{C}$
- 9:   **if**  $|\mathcal{K}| \geq 25$  **then**
- 10:     **return** first 25 concepts of  $\mathcal{K}$
- 11:   **end if**
- 12: **end for**
- 13: **raise error** ▷ unreached in practice

---

serves as a prototype representation of the class.  
Concepts are ranked by cosine similarity

$$s_i = \langle t_i, \mu_I \rangle.$$

To preserve semantic diversity, concepts are greedily selected while enforcing

$$\max_{k < i} \langle t_i, t_k \rangle < 0.80.$$

This removes near-duplicate concepts in the CLIP embedding space while favoring those that align with the visual distribution of the class.

### A1.5. Iterative Generation Procedure

Algorithm 1 summarizes vocabulary generation. Early rounds apply both lexical and CLIP-based filtering to encourage visual relevance and diversity. If a class has not reached 25 concepts after the CLIP-filtered rounds, later rounds disable CLIP pruning and keep only the lexical constraints, guaranteeing exactly 25 valid concepts per class.

### A1.6. CLIP-Based Concept Map Construction

After constructing the class-specific concept vocabulary (Sec. A1), we use CLIP to localize each concept within an image and build spatial concept maps. The goal is to measure how strongly each concept aligns with different spatial regions of the image.

**CLIP model.** We use a pretrained CLIP vision–language model to compute similarity between image regions and concept text prompts. In our implementation we use the ViT-B/16 architecture, loaded either through the `open_clip` library with pretrained weights (e.g., `laion2b_s34b_b88k`) or the original OpenAI CLIP implementation when `open_clip` is unavailable. All image

and text features are  $\ell_2$  normalized before computing cosine similarity.

**Concept text embeddings.** For each concept  $c_i$  in the vocabulary of size  $M = 25$ , we construct a CLIP text prompt using the template

$$t_i = \text{“a photo of } c_i \text{”}.$$

The CLIP text encoder produces a normalized embedding

$$\mathbf{t}_i = f_{\text{text}}(t_i) \in \mathbb{R}^D.$$

All text embeddings are precomputed and cached to avoid redundant computation during image processing.

**Spatial probing via localized prompts.** To obtain spatially localized responses, we probe the image using a grid of visual prompts. Each input image is first resized and center-cropped to the standard CLIP resolution of  $224 \times 224$ . We then define a uniform grid of  $H_t \times W_t$  spatial locations (typically  $7 \times 7$ ). For each grid cell center, we overlay a thin red circular outline with fixed radius  $r$  on the image.

This produces a set of  $H_t W_t$  modified images:

$$\{I_p\}_{p=1}^{H_t W_t},$$

where each  $I_p$  highlights a different spatial location through the circle prompt.

Each prompted image is encoded by the CLIP image encoder:

$$\mathbf{v}_p = f_{\text{img}}(I_p) \in \mathbb{R}^D.$$

The resulting features are also  $\ell_2$  normalized.

**Concept similarity maps.** For each spatial location  $p$  and concept  $i$ , we compute the cosine similarity between the image embedding and the concept embedding:

$$S_{p,i} = \mathbf{v}_p^\top \mathbf{t}_i.$$

Optionally, the similarity scores are scaled by the CLIP temperature parameter  $\exp(\text{logit\_scale})$ .

The resulting similarity tensor

$$S \in \mathbb{R}^{H_t W_t \times M}$$

is reshaped into a spatial concept map

$$P_i \in \mathbb{R}^{H_t \times W_t}$$

for each concept  $i$ . The stack of maps

$$P = \{P_i\}_{i=1}^M$$

represents the spatial activation of all concepts across the image.

## A2. Optimization Details

This section gives the solver details for the basis-learning objective (Eq. 1) and the inference problem (Eq. 3) in the main paper.

**Basis update.** We enforce non-negativity in Eq. 1 with the projected gradient step

$$\mathbf{W} \leftarrow \max(0, \mathbf{W} - \eta \nabla_{\mathbf{W}} \mathcal{L}_{\text{recon}}), \quad (\text{A2})$$

initialized with NNDSVD [4] for stable, accelerated convergence. With  $\mathbf{S}$  fixed,  $\mathcal{L}_{\text{recon}}$  is a smooth quadratic in  $\mathbf{W}$ , so projected gradient descent converges to a stationary point.

**Inference solver.** For the inference problem (Eq. 3), a fast non-negative initialization is the projected normal equation

$$\hat{\mathbf{S}}_0 = \text{ReLU}(\bar{\mathbf{A}}\mathbf{W}(\mathbf{W}^\top\mathbf{W})^{-1}), \quad (\text{A3})$$

optionally refined by projected gradient descent,

$$\hat{\mathbf{S}} \leftarrow \text{ReLU}\left(\hat{\mathbf{S}} - \eta(\hat{\mathbf{S}}\mathbf{W}^\top\mathbf{W} - \bar{\mathbf{A}}\mathbf{W})\right), \quad (\text{A4})$$

where the step size  $\eta$  is set from the spectral norm of  $\mathbf{W}^\top\mathbf{W}$ .

**Heatmap normalization.** For visualization, each concept channel is rescaled to  $[0, 1]$ ,

$$\mathbf{M}_k = \text{Normalize}\left(\hat{\mathbf{S}}_{\text{spatial}}(:, :, k)\right). \quad (\text{A5})$$

## A3. PGD Convergence Analysis

We analyze the convergence of the projected gradient descent (PGD) procedure used to optimize the activation-level reconstruction objective introduced in Sec. 3.4 of the main paper. In our formulation the semantic coefficient matrix  $\mathbf{S}$  is fixed, and we learn only the nonnegative concept basis  $\mathbf{W}$ .

Let  $\bar{\mathbf{A}} \in \mathbb{R}^{N \times p}$  denote the unfolded encoder activations, where  $N = nhw$  corresponds to the number of spatial locations across all images. The matrix  $\mathbf{S} \in \mathbb{R}^{N \times r}$  represents the fixed CLIP-derived semantic similarity matrix. The optimization problem for the concept basis  $\mathbf{W} \in \mathbb{R}_+^{p \times r}$  is

$$\min_{\mathbf{W} \geq 0} \mathcal{L}(\mathbf{W}) = \frac{1}{2} \|\bar{\mathbf{A}} - \mathbf{S}\mathbf{W}^\top\|_F^2. \quad (\text{A6})$$

This objective enforces activation-level fidelity between the original latent activations  $\bar{\mathbf{A}}$  and the reconstruction  $\mathbf{S}\mathbf{W}^\top$  obtained from the concept coefficients  $\mathbf{S}$  and concept bases  $\mathbf{W}$ .

**Smoothness.** The loss in Eq. A6 is a convex quadratic function of  $\mathbf{W}$ . Rewriting the objective as

$$\mathcal{L}(\mathbf{W}) = \frac{1}{2} \|\bar{\mathbf{A}}^\top - \mathbf{W}\mathbf{S}^\top\|_F^2,$$

its gradient with respect to  $\mathbf{W}$  is

$$\nabla_{\mathbf{W}} \mathcal{L}(\mathbf{W}) = \mathbf{W}(\mathbf{S}^\top\mathbf{S}) - \bar{\mathbf{A}}^\top\mathbf{S}. \quad (\text{A7})$$

Since  $\mathbf{S}^\top\mathbf{S}$  is positive semidefinite, the gradient is Lipschitz continuous with constant

$$L_{\nabla} = \|\mathbf{S}^\top\mathbf{S}\|_2. \quad (\text{A8})$$

Therefore the objective  $\mathcal{L}(\mathbf{W})$  is  $L_{\nabla}$ -smooth.

**Projected gradient update.** To enforce the nonnegativity constraint on  $\mathbf{W}$ , we apply projected gradient descent. The update rule is

$$\mathbf{W}_{k+1} = \Pi_{\mathbb{R}_+^{p \times r}}(\mathbf{W}_k - \eta \nabla \mathcal{L}(\mathbf{W}_k)), \quad (\text{A9})$$

where  $\Pi_{\mathbb{R}_+^{p \times r}}(\cdot)$  denotes the Euclidean projection onto the nonnegative orthant, implemented elementwise as  $\max(0, \cdot)$ .

**Descent property.** For an  $L_{\nabla}$ -smooth function, the standard descent lemma gives

$$\mathcal{L}(\mathbf{W}') \leq \mathcal{L}(\mathbf{W}) + \langle \nabla \mathcal{L}(\mathbf{W}), \mathbf{W}' - \mathbf{W} \rangle + \frac{L_{\nabla}}{2} \|\mathbf{W}' - \mathbf{W}\|_F^2. \quad (\text{A10})$$

Applying Eq. A10 with  $\mathbf{W}' = \mathbf{W}_{k+1}$  and using the optimality condition of the projection step yields

$$\langle \nabla \mathcal{L}(\mathbf{W}_k), \mathbf{W}_{k+1} - \mathbf{W}_k \rangle \leq -\frac{1}{\eta} \|\mathbf{W}_{k+1} - \mathbf{W}_k\|_F^2. \quad (\text{A11})$$

Substituting this bound into Eq. A10 gives

$$\mathcal{L}(\mathbf{W}_{k+1}) \leq \mathcal{L}(\mathbf{W}_k) - \left(\frac{1}{\eta} - \frac{L_{\nabla}}{2}\right) \|\mathbf{W}_{k+1} - \mathbf{W}_k\|_F^2. \quad (\text{A12})$$

Therefore, for any step size satisfying

$$0 < \eta < \frac{2}{L_{\nabla}}, \quad (\text{A13})$$

the objective decreases monotonically,

$$\mathcal{L}(\mathbf{W}_{k+1}) \leq \mathcal{L}(\mathbf{W}_k).$$

**Convergence.** Because  $\mathcal{L}(\mathbf{W}) \geq 0$ , the sequence  $\{\mathcal{L}(\mathbf{W}_k)\}$  is monotonically decreasing and therefore convergent. Furthermore,

$$\|\mathbf{W}_{k+1} - \mathbf{W}_k\|_F \rightarrow 0.$$

Every accumulation point of the PGD iterates satisfies the first-order optimality condition for Eq. A6. Since the

objective is convex and the feasible set  $\{\mathbf{W} \geq 0\}$  is convex, any such stationary point is a global minimizer of the problem.

#### A4. Additional Backbones

To test whether LAD’s behavior is consistent across encoder architectures, we evaluate four additional ImageNet backbones spanning different design families: RegNetY-8GF, ResNet-152, ResNeXt-50 (32×4d), and MobileNetV3-Large (Tab. A1). All methods use identical preprocessing, data splits, and concept count ( $r=25$ ).

**Consistency with the main results.** The pattern matches the main paper. LAD preserves reconstruction accuracy ( $\text{Acc} \geq 0.999$  on all four) and attains the highest or tied concept insertion (C-Ins) on every backbone, so its named concepts remain the most efficient at restoring the prediction. On deletion (C-Del), LAD and FACE trade the lead, as on ImageNet and Places365: LAD leads on RegNetY-8GF, while FACE edges it on ResNet-152 and ResNeXt-50. The gap is small in every case, consistent with LAD recovering a named, decision-relevant subset of the evidence FACE absorbs through unconstrained logit alignment.

**Robustness on a lightweight backbone.** MobileNetV3-Large is the most informative case. LAD remains stable ( $\text{Acc} 0.999$ ,  $\text{C-Ins} 0.962$ ,  $\text{C-Del} 0.946$ ), whereas CRAFT and FACE degrade sharply and become highly unstable across classes ( $\text{C-Del} 0.804 \pm 0.25$  and  $0.781 \pm 0.22$  versus LAD’s  $0.946$ ). Fixing the coefficients to language-grounded concepts evidently regularizes the decomposition on compact, low-redundancy architectures where the baselines’ jointly-optimized factors do not reliably converge.

#### A5. Second Clinical Domain: Dermoscopy

To test whether LAD’s clinical results extend beyond retinal fundus, we add a second medical domain, skin-lesion dermoscopy (HAM10000), explained with the same domain-matched medical CLIP (BiomedCLIP) used for fundus.

**Setup.** HAM10000 contains 10,015 dermoscopy images across seven lesion classes, split at the lesion level (all shots of a lesion kept together to prevent leakage) into 8,021 train / 1,994 validation (seed 42). The explained model is a ConvNeXt-Small with an ImageNet-pretrained encoder and a  $768 \rightarrow 7$  linear head, trained at 224 then fine-tuned at 448 with inverse-frequency-weighted cross-entropy and selected by balanced accuracy, reaching 0.846 balanced accuracy (0.878 top-1). Concepts are generated as in Sec. A1 (25/class, gpt-4o-mini) and localized with BiomedCLIP by red-circle prompting; full setup is in Tab. A3.

Table A1. LAD across four additional ImageNet backbones ( $r=25$ , identical splits). LAD leads or ties Acc and C-Ins on all four; LAD and FACE trade the deletion lead, as in the main paper. On MobileNetV3-Large the baselines become unstable (large per-class std), while LAD remains stable. Best C-Del per backbone in bold. All metrics  $\uparrow$ .

Backbone	Method	Acc	C-Ins	C-Del
RegNetY-8GF	LAD	1.000	0.977	<b>0.953</b>
	CRAFT	0.997	0.971	0.940
	FACE	0.998	0.977	0.951
ResNet-152	LAD	0.999	0.975	0.914
	CRAFT	0.995	0.971	0.867
	FACE	0.995	0.975	<b>0.952</b>
ResNeXt-50 (32×4d)	LAD	1.000	0.972	0.867
	CRAFT	0.992	0.963	0.861
	FACE	0.992	0.974	<b>0.961</b>
MobileNetV3-Large	LAD	0.999	0.962	<b>0.946</b>
	CRAFT	0.839	0.805	0.804
	FACE	0.856	0.813	0.781

**Results.** Table A2 reports concept faithfulness on both clinical domains under identical metric code and a matched  $7 \times 7$  probe grid, so differences reflect the concept basis rather than the evaluation. As on retinal fundus, accuracy saturates and LAD leads concept deletion (C-Del), exceeding the strongest baseline on dermoscopy (0.418 vs. CRAFT 0.366); LAD also retains saturated insertion (0.980) whereas FACE’s drops to 0.790. Absolute C-Del, however, is far lower than on fundus (0.418 vs. 0.954) for every method.

**Where the concepts localize.** Figure A1 explains the lower deletion score. The named concepts localize predominantly to the lesion *border* and peri-lesional skin rather than to the diagnostic lesion *interior*. For melanocytic nevus, “skin irregularity” and “irregular shape” form a ring around the lesion edge while the pigmented center stays inactive; for vascular lesion, “fluid filled,” “thin membrane,” and “mottled appearance” encircle the rim; for melanoma, “surrounding redness” and “scaly patches” fall on the margin and adjacent skin. Basal cell carcinoma is the main exception, with concepts landing on the lesion body. This boundary bias and the low C-Del are the same phenomenon: because the discriminative interior texture (pigment network, color variegation) is largely untouched, removing the boundary-localized concepts leaves the evidence the head relies on intact, so the prediction changes little. We report this as a limitation: in this domain LAD’s named concepts are spatially coherent and consistent across images, but they often track lesion shape and context rather than the internal morphology a dermatologist weighs most, so the explanations are better read as localizing *where* the model’s lesion-

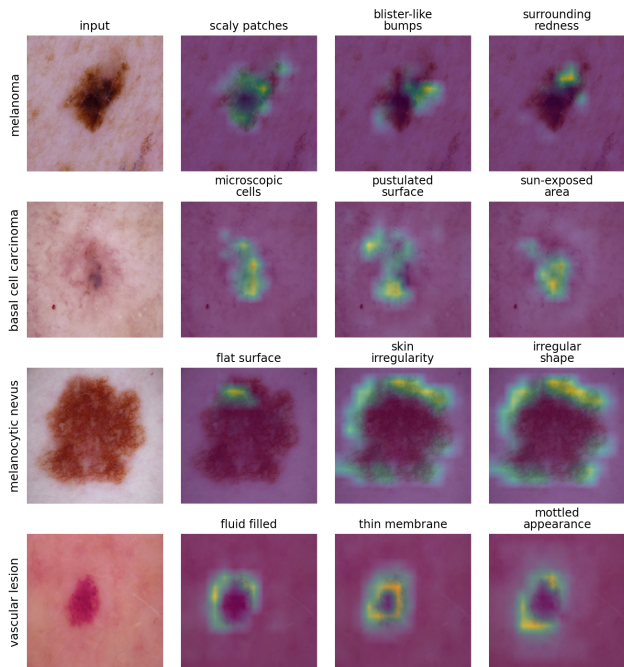


Figure A1. **LAD concepts on dermoscopy (HAM10000, BiomedCLIP)**. Top concepts for four lesion classes. The maps are spatially coherent and consistent but localize mainly to the lesion *boundary* and surrounding skin (e.g., “irregular shape” and “skin irregularity” ringing the nevus; “fluid filled”/“thin membrane” encircling the vascular lesion) rather than the diagnostic interior, with basal cell carcinoma a partial exception. This boundary bias is consistent with the lower concept-deletion score in this domain (Tab. A2).

Table A2. Concept faithfulness across two clinical domains (both BiomedCLIP,  $r=25$ ) under identical metric code. LAD leads C-Del in both. Dermoscopy uses a matched  $14 \times 14$  probe grid for all methods; absolute C-Del is lower on dermoscopy, where the concepts localize to the lesion boundary rather than its interior (Fig. A1). All metrics  $\uparrow$ ; best C-Del per domain in bold.

Domain	Method	Acc	C-Ins	C-Del
Retinal fundus	LAD	1.000	0.980	<b>0.954</b>
	FACE	0.990	0.980	0.863
	CRAFT	1.000	0.980	0.850
	ICE	0.990	0.980	0.455
Dermoscopy	LAD	1.000	0.980	<b>0.418</b>
	CRAFT	0.980	0.940	0.366
	FACE	0.990	0.790	0.254

level evidence sits than as asserting clinically complete reasoning.

## A6. Computational Cost

Table A4 breaks down the per-class cost of LAD on an RTX A4500 (ResNet34,  $r=25$ ). The recurring concept-

Table A3. Dataset, backbone, and concept-discovery setup for the two clinical domains. Both backbones are ImageNet-pretrained, head-replaced, trained at 224 then fine-tuned at 448 with weighted cross-entropy and balanced-accuracy selection; both use BiomedCLIP for concept localization.

	Retinal	Dermoscopy
Dataset	ODIR-5K	HAM10000
Classes	5	7
Train / Val	3,376 / 843	8,021 / 1,994
Backbone	DenseNet-121	ConvNeXt-Small
CLIP	BiomedCLIP	BiomedCLIP
Probe grid	$14 \times 14$	$14 \times 14$
PGD steps	250	150
Bal. acc.	0.755	0.846

learning cost, the basis fit, is 0.03 s, an order of magnitude below CRAFT (0.5 s) and FACE (2.6 s), because fixing  $\mathbf{S}$  reduces basis learning to a single non-negative least-squares solve rather than alternating factor updates. Inference is effectively free. The dominant cost is CLIP concept-map construction, a one-time, fully cacheable preprocessing step; the LLM vocabulary is generated once ( $\sim 15$  s/class) and cached.

Table A4. Per-class cost on an RTX A4500 (ResNet34,  $r=25$ ). The recurring fit is the concept-basis solve, where LAD is far faster than the baselines. CLIP map construction and LLM vocabulary are one-time, cacheable preprocessing. Memory is peak GPU during each stage.

Stage	Wall (s)	GPU peak (MB)
Activation extraction	0.01	926
CLIP map construction	6.45	1729
LLM vocab (one-time)	15.0	0
LAD fit	<b>0.03</b>	745
LAD inference	< 0.01	722
CRAFT fit	0.50	783
FACE fit	2.60	795

**CLIP map construction is the bottleneck, and it is bounded.** Concept-map construction probes a  $14 \times 14$  grid of red-circle prompts per image, so its cost scales with the number of CLIP forward passes, not with the decomposition. It is also the only memory-significant stage. Table A5 shows peak GPU memory as a function of CLIP batch size: the whole pipeline fits in under 1.8 GB even at the default batch, with throughput around 1,000 prompted variants per second. The step is parallel across grid locations and images and is computed once per class, then cached.

**Grid sensitivity.** The probe grid sets both the spatial resolution of the concept maps and the cost. Table A6 com-

Table A5. CLIP map construction: peak GPU memory and throughput versus batch size ( $14\times 14$  grid, RTX A4500). Memory grows gracefully with batch; the pipeline default (196, one full grid per image) peaks under 1.8 GB.

CLIP batch	GPU peak (MB)	Variants/s
16	976	1158
32	1045	1156
64	1183	988
128	1450	1032
196	1729	970

compares the  $7\times 7$  grid (used for ImageNet and dermoscopy) with the  $14\times 14$  grid (used for the retinal fundus models). The finer grid quadruples the prompted variants per image ( $49 \rightarrow 196$ ) and costs roughly  $3.4\times$  the time and  $1.6\times$  the peak memory, the price paid for the higher-resolution localization that focal retinal evidence benefits from.

Table A6. Grid sensitivity of CLIP map construction (32 images, RTX A4500). The  $14\times 14$  grid used for retinal fundus costs more than the  $7\times 7$  grid but yields higher-resolution concept maps.

Grid	Variants/img	Wall (s, 32 img)	GPU peak (MB)
$7\times 7$	49	1.88	1116
$14\times 14$	196	6.37	1737

## A7. Vision Transformer Case Study

NMF-style concept discovery (ICE, CRAFT, FACE) is formulated for convolutional feature maps: it factorizes a spatial activation tensor whose channels share a consistent, translation-equivariant geometry. Vision Transformers break both assumptions, they emit patch tokens rather than a spatial map, mix global information through self-attention at every layer, and route the prediction through a [CLS] token rather than pooled spatial features. Consequently no existing post-hoc concept-discovery method is designed to operate on both CNNs and ViTs, and the convolutional baselines do not apply to patch tokens at all. Because LAD fixes language-grounded coefficients and learns only a basis, it can be *run* on ViT patch tokens without modification, which lets us ask a question the field has not examined: when an anchored decomposition is applied to a transformer, *what kind of concepts does it actually recover?*

**Setup.** We decompose the penultimate patch-token representation of ViT-B/16 ( $14\times 14\times 768$ ) into the language-anchored basis and let the remaining block, LayerNorm, and head complete the forward pass, on the same 500 ImageNet classes ( $r=25$ ).

### Reconstruction transfers, but localization does not.

Numerically, the decomposition reconstructs the representation well: reconstruction accuracy and concept insertion are saturated ( $\text{Acc} = 0.98$ ,  $\text{C-Ins} = 0.98$ ). Concept deletion, however, is near zero ( $\text{C-Del} = 0.02$ ). Two factors combine here. First, the head reads from the preserved [CLS] token, which carries information from the original forward pass, so ablating patch-token concepts has little effect on the logits, and CNN-style deletion is not directly meaningful. Second, and more telling, the recovered concept maps are weakly localized.

Figure A2 makes this visible. On CNNs, LAD localizes named concepts to the corresponding object part (Sec. 5.1, main paper); on ViT, the same concepts spread diffusely and frequently attach to the *background* or trace the object *silhouette* rather than the named part. “Cold blooded” for the crocodile activates on the surrounding rock and water; “large ears” on the elephant covers the whole head and contour rather than the ears; the bear’s “hunting stance” and “playful cubs” fire across the entire frame. A few color- or texture-defined concepts do localize (“yellow peel” and “ripe fruit” on the banana), but the part- and pose-level concepts that localize cleanly on CNNs do not. The maps behave closer to global saliency or edge responses than to the part-grounded evidence LAD recovers on convolutional encoders.

**Takeaway.** This is a negative result, and an informative one: it shows *why* spatial concept decomposition is not readily transferable to transformers. The patch-token geometry, global attention mixing, and [CLS]-routed prediction together mean that a language-anchored basis can reconstruct the representation (high insertion) without its concepts being spatially faithful (low deletion, diffuse maps). A transformer-native formulation, operating on the [CLS] attention pathway rather than patch tokens, and a [CLS]-aware deletion protocol, are needed before concept discovery is meaningful on ViTs; we view this as the natural next step rather than a property of LAD specifically.

Table A7. LAD on ViT-B/16, 500 ImageNet classes,  $r=25$ . The anchored decomposition reconstructs the representation ( $\text{Acc}$ ,  $\text{C-Ins}$  saturated) but its concepts are not spatially faithful: deletion is near zero and the maps are diffuse (Fig. A2).  $\text{C-Del}$  is not comparable to the CNN setting under the preserved [CLS] pathway.

Backbone	Acc $\uparrow$	C-Ins $\uparrow$	C-Del
ViT-B/16	0.98	0.98	0.02 $\dagger$

$\dagger$  Not comparable to CNNs (preserved [CLS] pathway; see text).

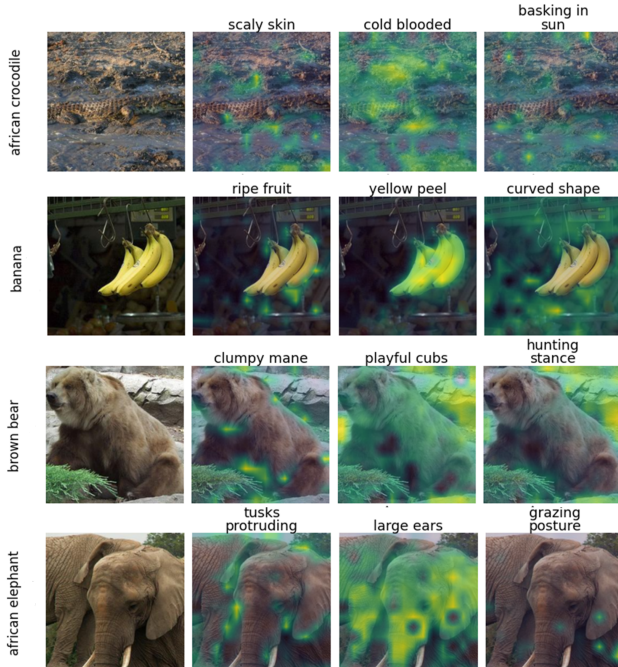


Figure A2. **LAD concepts on ViT-B/16.** For four ImageNet classes, the top language-anchored concepts on patch tokens. Unlike the part-level localization LAD produces on CNNs (Sec. 5.1, main paper), the ViT maps are diffuse and often attach to background or to the object silhouette rather than the named part (e.g., “cold blooded” on surrounding rock, “large ears” over the whole head). Color- and texture-defined concepts localize better (“yellow peel”). The maps behave closer to global saliency than to part-grounded evidence, illustrating why spatial concept decomposition does not transfer directly to transformers.

## A8. Visual analysis of concept maps

The concept visualizations in Figures A3–A5 demonstrate that our method discovers interpretable and spatially grounded concepts across a diverse range of ImageNet categories. For object-centric classes such as *Ambulance*, the model captures distinctive parts including “Ambulance Text,” “Front Grille,” with heatmaps closely aligned to the corresponding regions of the vehicle. Contextual cues such as “Urban Street Setting” and “Paramedics Nearby” also emerge, reflecting the model’s ability to represent both object parts and scene-level signals.

For natural categories like *Bald Eagle*, the discovered concepts emphasize fine-grained attributes such as “Sharp Talons,” “Wide Wingspan,” “Tail Feathers Spread,” and “Perched on Branch,” demonstrating that the factorization captures species-dependent morphology and pose-specific details.

The *Banana* and *Basketball* classes similarly exhibit semantically coherent concepts: color and ripeness cues

(“Ripe Spot,” “Yellow Peel”), cluster structure (“Hanging Bunch”), and environment attributes (“Crowd in the Background,” “Court Floor Line,” “Player Shoes”). These maps show that the method cleanly separates object features from contextual scene information.

Finally, the *Church* and *Electric Guitar* classes highlight the model’s ability to encode structural and material properties. Concepts such as “Brick Exterior,” “Bell Tower,” and “Interior Chandeliers” reflect architectural components, while guitar-related concepts such as “Fret Markers,” “Metal Strings,” “Musician Posture,” and “Stage Lighting” localize on instrument parts and performance settings.

Overall, these qualitative results illustrate that the proposed model recovers rich, human-understandable concepts that respect object structure, texture, and scene context, providing spatially faithful explanations without manual labeling.

## A9. Additional Concept Discovery Comparison

Figure A6 provides further qualitative comparisons across both ImageNet and Places365. ICE, CRAFT, and FACE typically focus on coarse object regions or isolated texture cues, often without semantic consistency across samples. In contrast, LAD discovers interpretable, localized, and semantically named concepts—such as part-level attributes, materials, textures, and scene elements—demonstrating clearer semantic grounding and improved interpretability across both object-centric and scene-centric datasets.

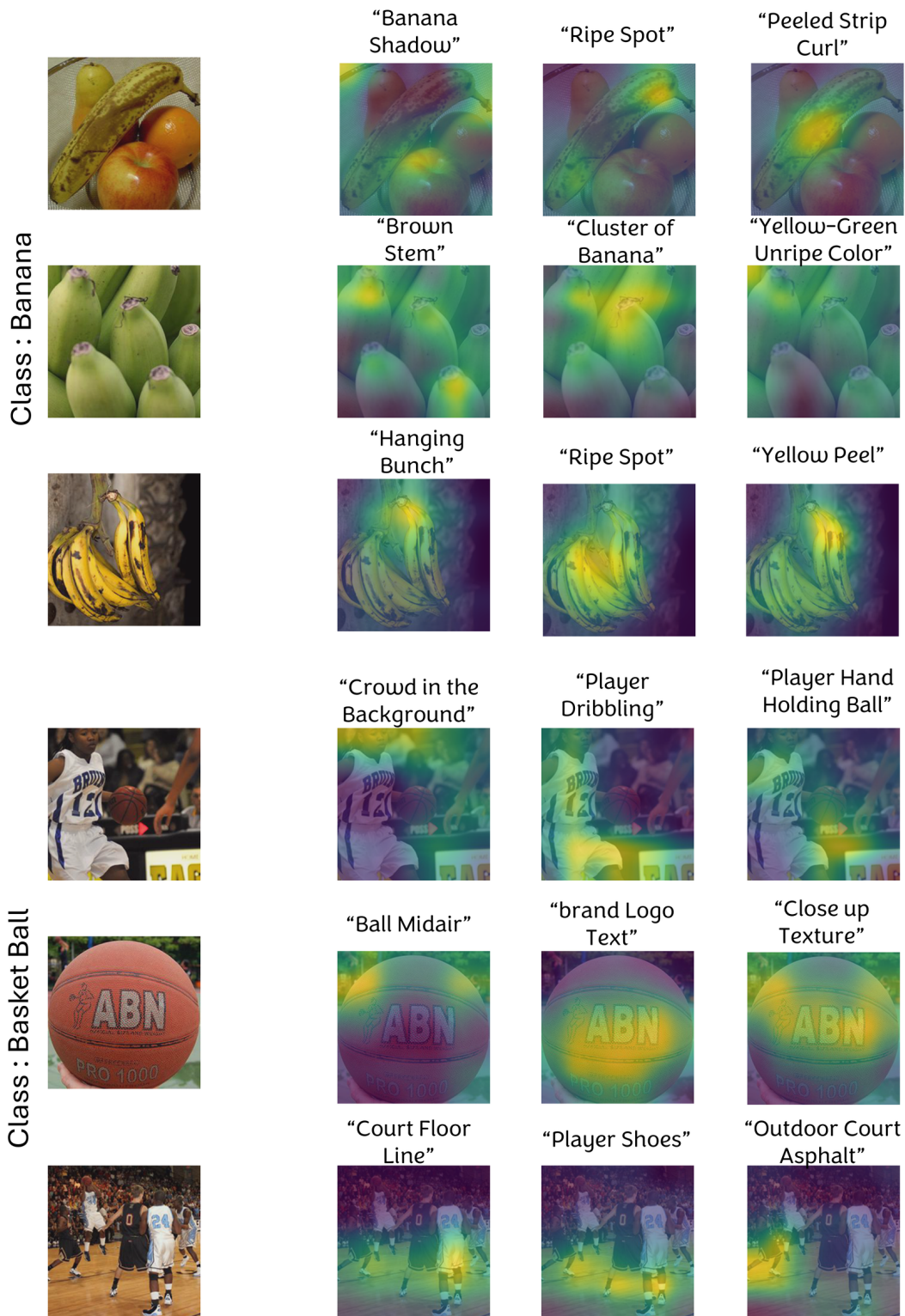


Figure A3. Concept maps for the Banana and Basketball classes, with the highest-activating learned concepts overlaid on input images.

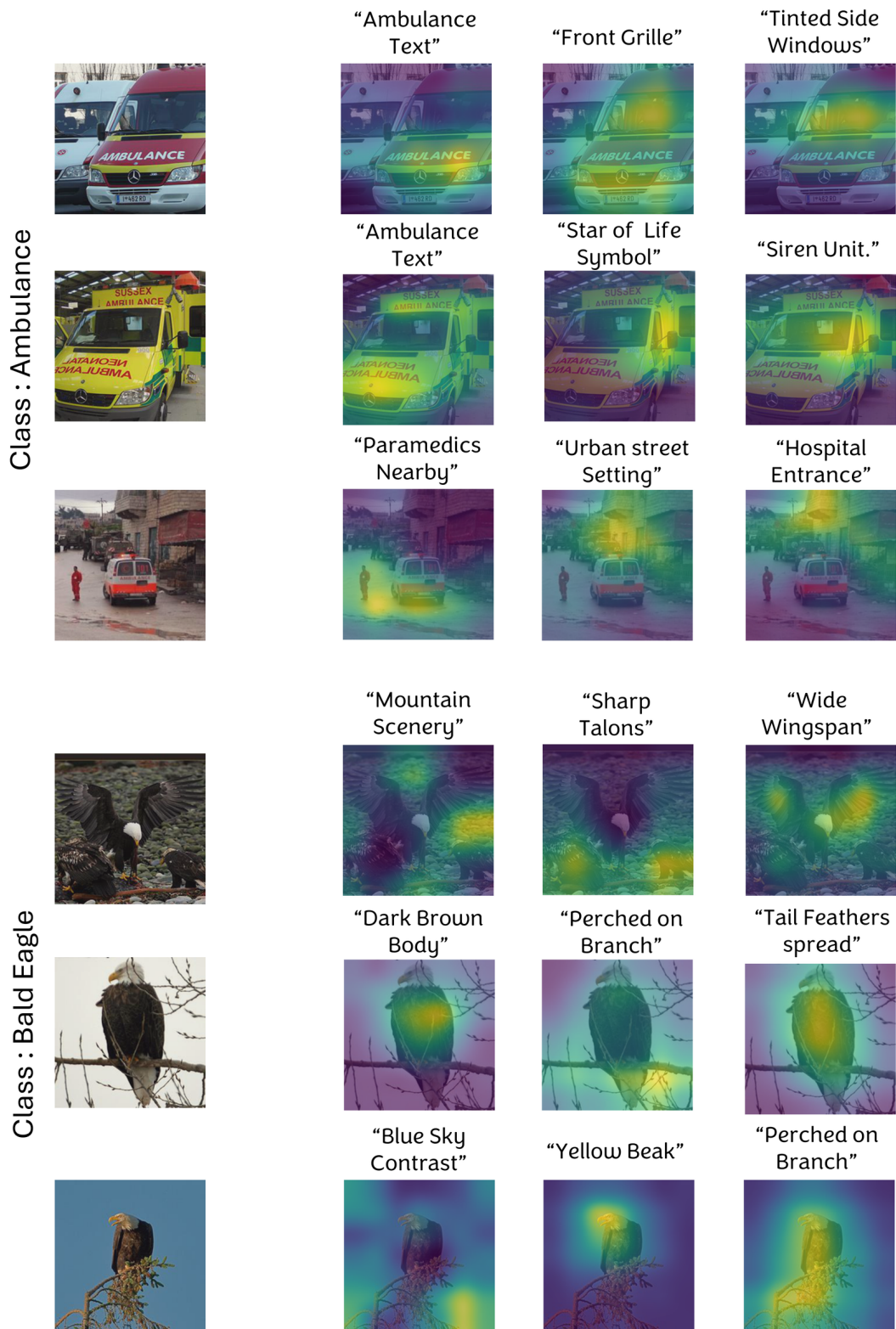


Figure A4. Concept maps for the Ambulance and Bald Eagle classes, showing input images and the top activated visual concepts.C

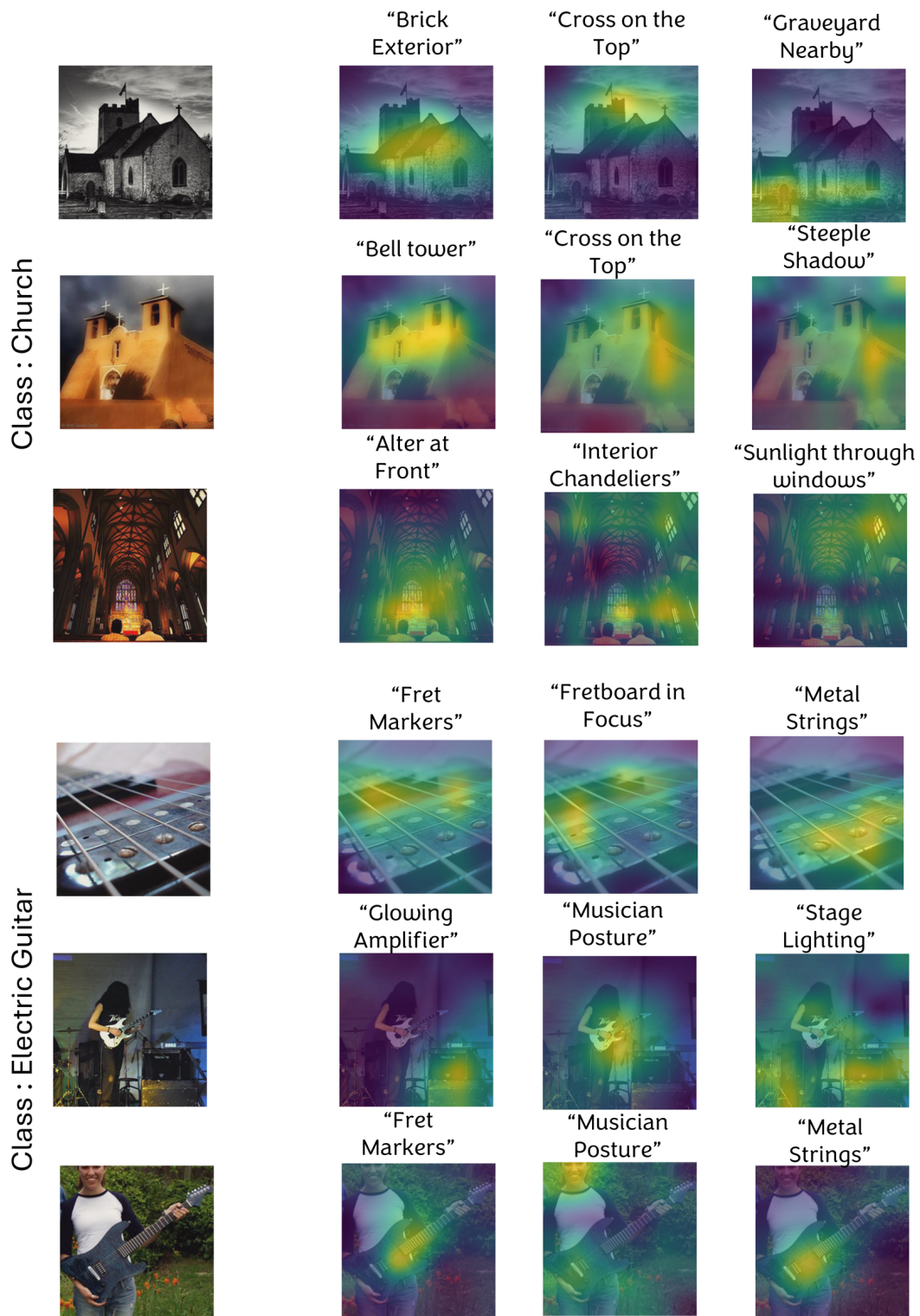
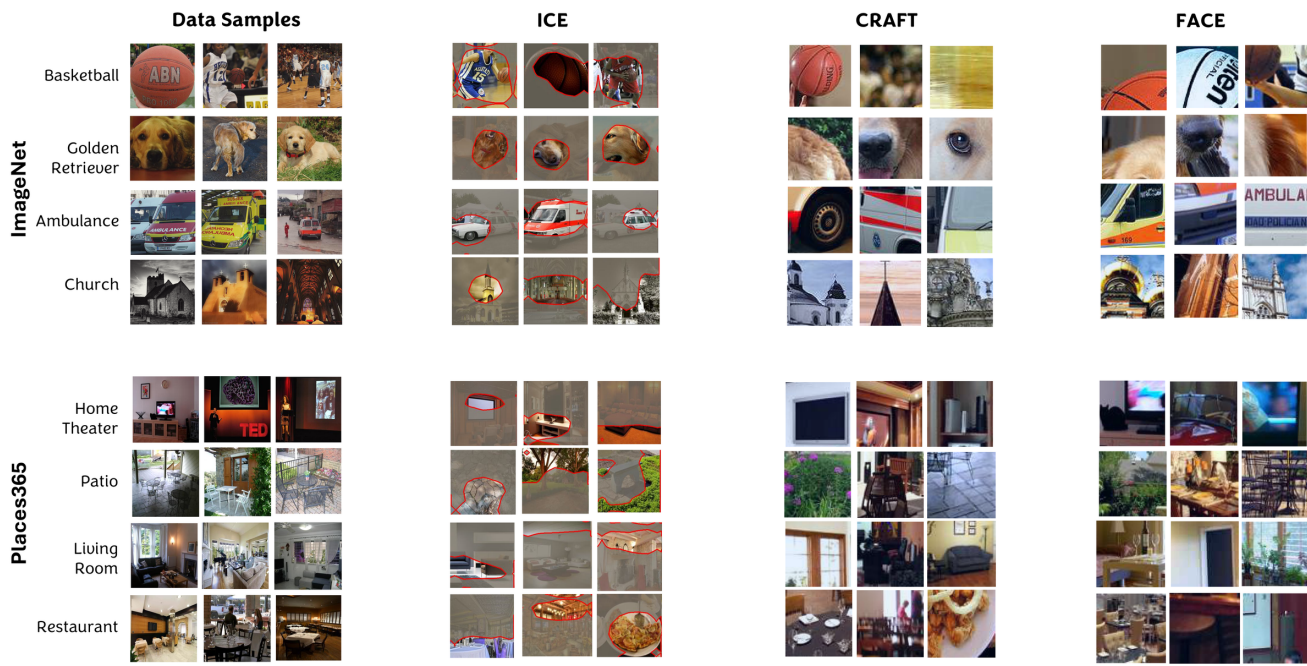


Figure A5. Concept maps for the Church and Electric Guitar classes, highlighting the learned part-, texture-, and context-level concepts.



**Language Anchored Decomposition Method**

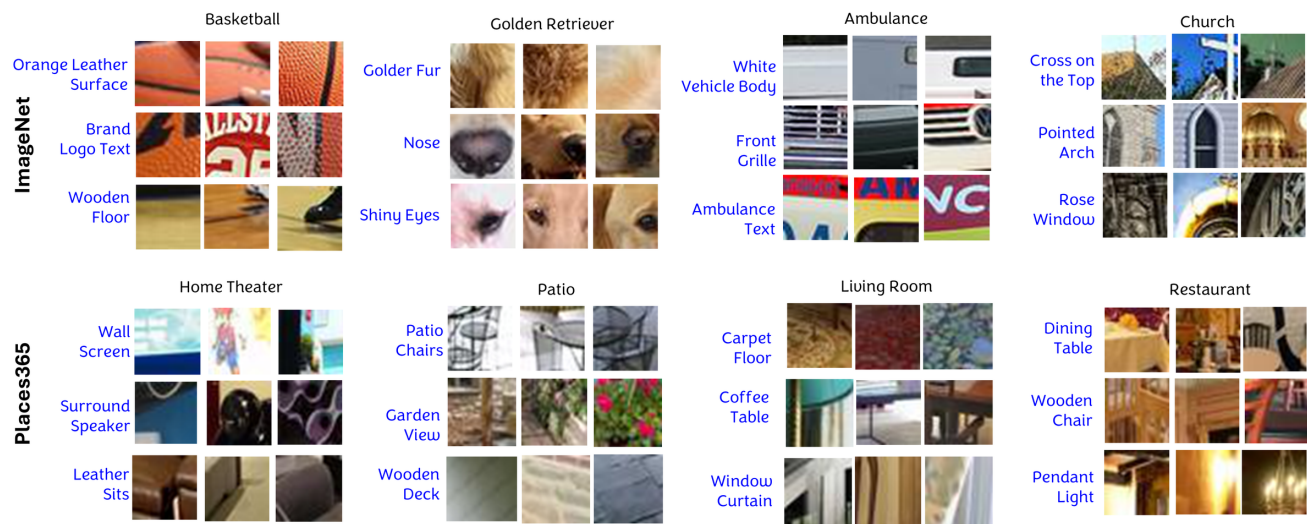


Figure A6. Additional qualitative comparison of concept discovery methods on ImageNet and Places365. For each class, we show representative input samples (left), followed by concepts extracted using ICE, CRAFT, and FACE, and the concepts discovered by LAD (bottom). Baseline methods highlight coarse or fragmented regions, while LAD identifies fine-grained, semantically meaningful, and spatially coherent concepts.